PHILOSOPHICAL TRANSACTIONS OF THE ROYAL SOCIETY A MATHEMATICAL, PHYSICAL & ENGINEERING SCIENCES

Process Modelling and Microstructure [and Discussion]

M. Rappaz, Ch.-A. Gandin, A. M. Stoneham, M. McLean and M. S. Loveday

Phil. Trans. R. Soc. Lond. A 1995 **351**, 563-577
doi: 10.1098/rsta.1995.0053

Process modelling and microstructure

By M. Rappaz and Ch.-A. Gandin

Ecole Polytechnique Fédérale de Lausanne, Laboratoire de métallurgie physique, MX-G, CH-1015 Lausanne, Switzerland

Among the many routes which are used for the processing of high-temperature materials, solidification plays a key role. Several modelling tools are now available for the simulation of the interconnected macroscopic phenomena associated with any casting process (heat exchange, mould filling, convection, stress development, etc.). Based upon finite-difference (FD) or finite-element (FE) techniques, these models solve the continuity equations of mass, energy, momentum, solute species, averaged over the liquid and solid phases. As such, macroscopic models do not account for the detailed phenomena occurring at the scale of the microstructure. For that reason, a stochastic cellular automaton (CA) model has been developed recently for the prediction of the grain structure formation in solidification processes, in particular during the investment casting of superalloys. Such a microscopic model considers the heterogeneous nucleation of grains at the surface of the mould and in the bulk of the liquid, the growth kinetics and preferential growth directions of the dendrites and the microsegregation. The microscopic CA model has been coupled to FE heat flow computations in order to predict the grain structure at the scale of a casting. It is shown that microstructural features and crystallographic textures can be simulated as a function of the casting conditions and alloy composition.

1. Introduction

Numerical simulation has been first used by civil and mechanical engineers for the calculation of deformation, fluid dynamics and heat transfer. Based upon finite-difference (FD) or finite-element (FE) methods, these models solve the continuity equations of heat, mass and momentum. These tools were then transferred and adapted to the field of materials science. Therefore, it is not surprising that most of these 'macroscopic' models are primarily concerned with macroscopic entities such as the temperature, stress, strain or velocity fields. In a given process such as forming or solidification, these fields (e.g. the temperature distribution) can be related to the process parameters (e.g. the heat flow extracted from a cooling system). Such information might be useful to the process engineer, but it is only an 'intermediate' output: the materials scientist is interested in the characteristics (microstructure/defects) and final mechanical/functional properties/performances of the product.

To predict entities which are of some relevance to materials scientists, two approaches can be used. The first one is based on empirical relationships or expert systems (e.g. neural networks) whose input can be either the process parameters

Phil. Trans. R. Soc. Lond. A (1995) **351**, 563–577
Printed in Great Britain

or the 'intermediate' output. This method is straightforward but does not bring much insight into the microscopic mechanisms. The second approach, which is more tedious, is to simulate the various microscopic phenomena which cannot be accounted for by a continuum model. Such a *micro-macroscopic* approach will be illustrated in the present paper for the particular case of the grain structure formation in solidification processes (Rappaz 1989).

Solidification is an important route for the production of many parts and components, in particular in aerospace applications (turbine blades, diffuser cases, vanes, etc.). Solidification is also an illustration of the manifold lengthscales that intervene in materials science (process scale (cm–m), grain size (mm), dendrites/eutectic spacings (μm), atomistic scale (< nm)). After a short review of the macroscopic models used in solidification processes (§ 2), this contribution will present a stochastic model recently developed for the prediction of nucleation and growth of dendritic grains (§ 3). The coupling of these two scales is discussed in § 4 and the last section outlines some of the future developments that will be made in this area.

2. Macroscopic modelling

(*a*) *Geometry description and enmeshment*

Three-dimensional (3D) components are described nowadays by computer-aided design (CAD) files coming from the designer. The engineer in charge of the production of the component via a casting process must first read this file and then add several other domains: risers, ingates, mould parts, insulation, cooling devices, etc. Using these CAD files, the corresponding volumes must be then enmeshed in order to solve the continuum equations. This is done with grid points or elements for the FD or FE methods, respectively. It is beyond the scope of the present paper to discuss the advantages and disadvantages of these two numerical techniques but the enmeshment procedure is still a critical step. Figure 1*a* shows the enmeshment of a structural aircraft component. Only half of the piece is shown together with the risers and gating.

(*b*) *Fraction of solid and solidification path*

Because of the fineness of the microstructure that develops during solidification, the macroscopic models do not track the position of the solid–liquid interface but rather use continuity equations averaged over the two phases (Bennon & Incropera 1987; Voller *et al.* 1989; Ganesan & Poirier 1990; Ni & Beckerman 1991). This averaging procedure introduces a new field: the volume fraction of solid, f_s. Since there is no additional continuity equation governing the evolution of this entity, a local relationship, the solidification path, has to be found between f_s and the temperature, T. Such a relationship is given by a local solute balance (microsegregation model) and by the phase diagram of the alloy. Most of the macroscopic models of solidification use a unique solidification path, $f_s(T)$, which range from a linear interpolation between the liquidus and solidus temperatures, to more sophisticated models such as the lever rule, the Scheil–Gulliver or the Brody–Flemings models (Kobayashi 1988). All these models apply to a closed system, i.e. when there is no fluid flow.

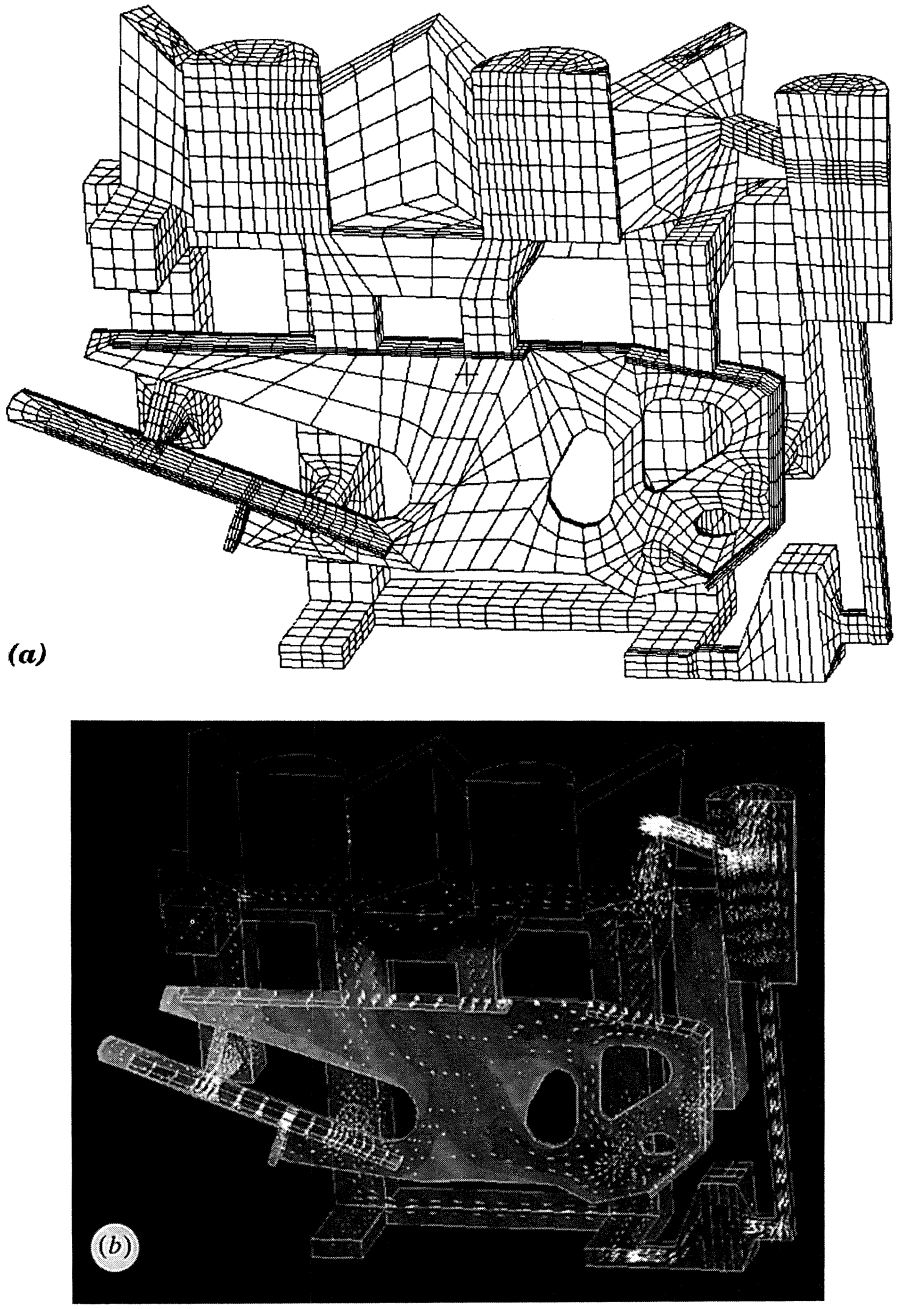

Figure 1. Structural aircraft component in Al-alloy (investment casting): (*a*) 3D enmeshment of a casting and (*b*) corresponding temperature and fluid flow velocities during mould filling (courtesy of CERCAST, calculation made with ProCAST^{TM}).

(*c*) *Heat and fluid flow calculations*

Even though the convection associated with pouring effects, buoyancy, surface tension gradients or electromagnetic forces modifies the local solute balance

PHILOSOPHICAL TRANSACTIONS OF THE ROYAL SOCIETY A MATHEMATICAL, PHYSICAL & ENGINEERING SCIENCES

made within a small volume element of the enmeshment, most of the simulation codes developed for solidification processes assume a unique $f_s(T)$ relationship. The averaging of the continuity equations is usually made under the assumption that the solid skeleton is fixed. The permeability, K, of the mushy zone is introduced to simulate the interdendritic flow in the porous medium constituted by the dendrites array (Darcy equation). Detailed derivations of these equations can be found, for example, in Bennon & Incropera (1987), Voller *et al.* (1989), Ganesan & Poirier (1990), Ni & Beckerman (1991). As an example, the temperature distribution and fluid flow velocities calculated within the component of figure 1*a* are shown in figure 1*b*. The results have been computed with the software ProCAST^{TM}, taking into account heat flow and fluid flow with free surface (mould filling).

(*d*) *Prediction of macro- and mesosegregation*

Macro- and mesosegregation, two defects frequently encountered in castings, are solute concentration inhomogeneities observed at the scale of the casting or at a more localized scale (e.g. segregated channels or freckles). Both types of segregation are associated with the transport of solute species by convection. Neglecting the diffusion of solute species at the macro- and mesoscales, the local solute concentration is averaged over the solid and liquid phases using a microsegregation model. The simplest model makes the assumption of local equilibrium between the solid and liquid phases (lever rule). Scheil or back-diffusion microsegregation models, which are closer to the case of real alloys, are more difficult to handle for systems in which convection occurs (Rappaz & Voller 1990; Mo 1994).

As a result of convection (open system), the local average concentration is no longer constant and the solidification path, $f_s(T)$, is no longer unique. For example, the arrival of solute-rich liquid can partly remelt the solid even though the local temperature is decreasing monotonically. This phenomenon is typically associated with solutal convection in the mushy zone and may lead to the formation of segregated channels or freckles. The simulation result shown in figure 2 corresponds to the formation of such an instability in a large rectangular two-dimensional (2D) ingot of Ni–Al (Combeau & Lesoult 1993).

3. Microstructure modelling

(*a*) *Nucleation of grains*

The formation of primary phase grains during solidification starts with the heterogeneous nucleation of nuclei at the surface of the mould or within the bulk of the liquid. Convection can also play a significant role at this stage since it can transport grains and enhance the density of nuclei by dendrite fragmentation (Sato *et al.* 1987). Such effects will be ignored in the investment casting of superalloys considered in the present paper. Although the theory of heterogeneous nucleation is fairly well known (Turnbull 1950), the mechanisms are still unclear. For that reason, most simulation approaches consider that the heterogeneous nucleation of grains is described by a distribution of nucleation sites, $p(\Delta T)$, which become active as the undercooling, ΔT, is increased (Rappaz 1989). The parameters of this distribution are determined by comparison with experimental results obtained under different cooling rates but identical inoculation conditions. The density of grains in the bulk of the liquid, $n(t)$, at a given time, t, is then given

PHILOSOPHICAL TRANSACTIONS OF THE ROYAL SOCIETY A MATHEMATICAL, PHYSICAL & ENGINEERING SCIENCES

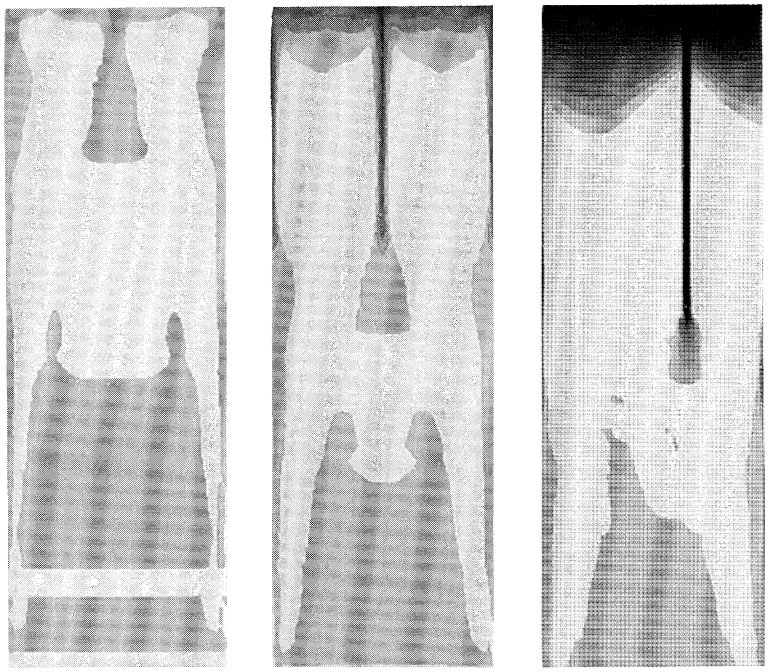

(*a*) (*b*) (*c*)

Figure 2. 2D Al concentration distribution and freckle formation in a large Ni–Al rectangular ingot after (*a*) 1 h, (*b*) 1 h 23 min and (*c*) 8 h (courtesy of Combeau *et al.* 1993).

by

$$n(t) = \int_0^{\Delta T(t)} p(\Delta T)(1 - f_s)\,\mathrm{d}(\Delta T). \tag{3.1}$$

The factor $(1 - f_s)$ accounts for the disappearance of the nucleation sites which are trapped by the grains already formed (Hunt 1984). Equation (3.1) has been used originally for the formation of equiaxed grains in the bulk of the liquid, but the same approach can be adapted to the heterogeneous nucleation at a mould surface (Rappaz & Gandin 1993).

(*b*) *Dendrite growth*

For the sake of simplicity, let us first consider the situation of a uniform temperature field. After a grain has nucleated, it grows first as a sphere, then becomes unstable and later grows with a dendritic morphology. The growth velocity of the tips of the dendrites, $v(\Delta T)$, is a function of the local undercooling and can be estimated using various analytical models (Kurz & Fisher 1989). For cubic metals, the growth directions of the dendrite trunks and arms correspond approximately to $\langle 100 \rangle$ crystallographic directions (Chalmers 1964). Thus, in a uniform temperature field, a grain grows almost as an octahedron whose diagonals are given by the $\langle 100 \rangle$ directions of the parent nucleus. The situation illustrated in figure 3 corresponds to 2D dendritic grains growing in a plane with a square shape. Neglecting the initial stage of spherical growth, the half-length of the $\langle 100 \rangle$ diagonals of the grains, $L(t)$, is given by

$$L(t) = \int_{t_n}^{t} v(\Delta T(t))\,\mathrm{d}t, \tag{3.2}$$

PHILOSOPHICAL TRANSACTIONS OF THE ROYAL SOCIETY A MATHEMATICAL, PHYSICAL & ENGINEERING SCIENCES

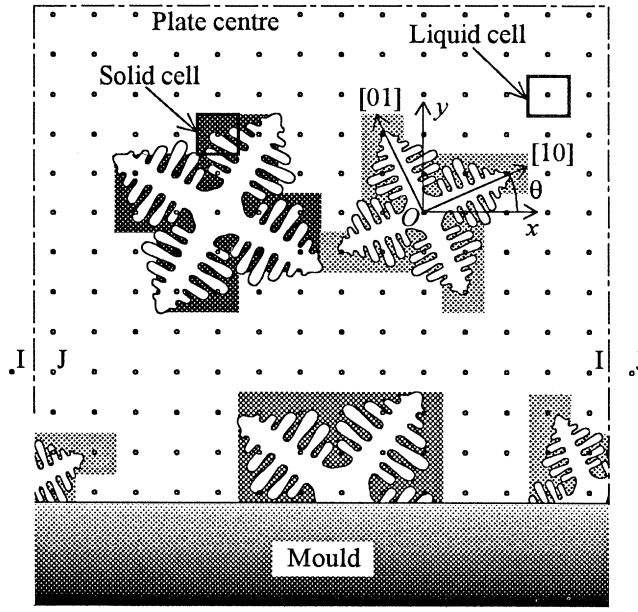

Figure 3. Schematic diagram of a 2D CA model for the nucleation/growth of grains in a uniform temperature field.

where t_n is the time of nucleation. Within the octahedron, the volume is mushy. A simple solute diffusion model can be used to predict the internal volume fraction of solid within the grains (Rappaz & Thévoz 1987).

Based upon these simple considerations, the simulation of grains growing in a thermal gradient can be calculated using the cellular automaton briefly described below (Rappaz & Gandin 1993; Gandin & Rappaz 1994).

(*c*) *Cellular automaton*

To predict the nucleation and growth of grains in any thermal environment, a physically based cellular automaton (CA) has been developed. For that purpose, the volume of the melt is divided into N_c regular square cells (figure 3). For each cell ν, a 'crystallographic' index, Ic_ν, is defined. It is equal to zero at the beginning of the simulation meaning that the cell is liquid. During solidification, this index can become a positive integer whose value corresponds to a given misorientation of the dendritic network with respect to the axes of the CA network. Furthermore, the cells which belong to the boundary of the domain are marked with an additional index and are referred to as 'boundary cells'.

For the nucleation in the bulk of the specimen, a certain number of nucleation undercoolings are randomly selected according to the pre-determined nucleation distribution $p(\Delta T)$ (e.g. Gaussian distribution). These undercoolings are spatially attributed to randomly chosen cells. The same procedure is applied to the boundary cells with the appropriate nucleation site distributions. All the cells which have been attributed a critical nucleation undercooling, $\Delta T_\nu^{\mathrm{nuc}}$, are referred to as 'nucleation cells' in the following.

Let us assume now that the cooling curve, $T_\nu(t)$, at any cell location is known. This cooling history can be obtained from the cooling curve measured in a small specimen of nearly uniform temperature (figure 3) or it can be calculated using FE

heat flow computations, as explained in more detail in § 4. During a time-stepping calculation, a cell ν can make a transition from the liquid state ($Ic_\nu = 0$) to a dendritic state ($Ic_\nu \geqslant 1$) according to two mechanisms.

1. If the cell is a nucleation cell and is still liquid at time t, it can become a new nucleus if its undercooling becomes larger than the predetermined critical nucleation undercooling (i.e. if $\Delta T_\nu(t) = T_\mathrm{L} - T_\nu(t) \geqslant \Delta T_\nu^{\mathrm{nuc}}$). Its index Ic_ν giving the crystallographic orientation of the new grain is set to a randomly selected value.

2. Once a cell has nucleated, the corresponding grain is assumed to grow with the kinetics of the dendrite tips, $v(\Delta T_\nu)$ (Kurz *et al.* 1986). In two dimensions, it grows as a small square envelope (see figure 3). At a certain time, the dendrite envelope reaches the centres of the four nearest-neighbour cells. If these neighbours are still liquid, their indices are set to the value of the parent nucleus thus taking on the orientation of the grain. The growth procedure is then repeated for the neighbouring cells using the corresponding local undercooling.

The simple 'capture' procedure of the cells which is described above has a major drawback: it propagates the growth of dendritic grains from cells to cells but it biases their misorientations. This problem is well known in the application of cellular automata and Monte Carlo methods to grain growth (Toffoli & Margolus 1991; Anderson *et al.* 1984). A 2D growth algorithm which does not present this drawback is described by Gandin & Rappaz (1994). This algorithm has not yet been extended to 3D situations. However, a simple octahedron growth algorithm has been used for uniform temperature situations in three dimensions (Gandin *et al.* 1993).

(*d*) *Results*

Figure 4 shows the grain contours seen in a transverse section of an equiaxed turbine blade airfoil (Gandin *et al.* 1994). The superalloy was cast at the SNECMA foundry in a ceramic mould coated with inoculant particles. The grain boundaries, clearly revealed by the etching procedure, were redrawn to produce the grain structure of figure 4*a*. The result of the simulation which is shown in figure 4*b* has been obtained using the 3D stochastic model under the assumption of a uniform temperature field. For that purpose, a small length of the blade normal to the 2D section was considered and the final grain structure is shown in the same transverse section. The label 'equiaxed blade' used in the investment casting industry for such grain structures is somehow misleading since the grains shown in the simulated micrograph were assumed to nucleate only at the surface of the ceramic mould (i.e. columnar growth starting from the surface). However, since the octahedral grains may grow at some angle with respect to the transverse section plane, many of them are not directly connected to the edge of the airfoil and thus appear as 'equiaxed'. This simple example shows how the results of a simple 3D stochastic growth model can provide useful stereological information.

This simple 3D growth model can also predict the grain competition that occurs within the columnar zone of a casting. Since the dendritic network is constrained to grow along ⟨100⟩ directions, the grains which have one of their ⟨100⟩ orientations most closely aligned with the thermal gradient direction are selected by the growth process at the expense of less favourably oriented grains (Chalmers 1964). As a result of this grain competition, the grain density measured in a section par-

PHILOSOPHICAL TRANSACTIONS OF THE ROYAL SOCIETY A MATHEMATICAL, PHYSICAL & ENGINEERING SCIENCES

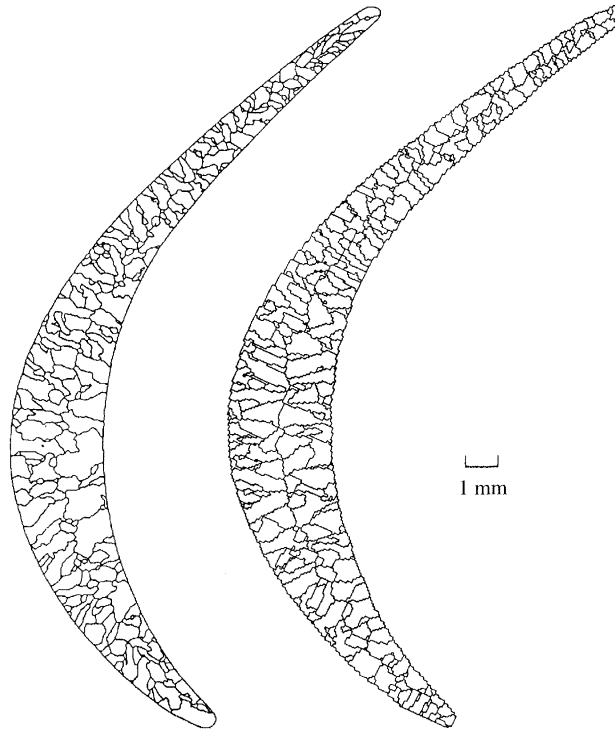

Figure 4. (*a*) Measured and (*b*) predicted grain structures in the cross section of an equiaxed turbine blade airfoil (Gandin *et al.* 1994).

allel to the surface of nucleation must decrease with the distance to this surface. This is shown in figure 5 for an Inconel X750 alloy (Gandin *et al.* 1995). This alloy was cast in a preheated ceramic mould attached to a copper chill plate. The mean linear grain boundary intercept normal to the growth direction was measured in a longitudinal section and is reported as a function of the distance to the chill. The same measurement was made for the grain structure computed with the 3D stochastic model. Although the assumption of uniform temperature made in the simulation is no longer valid near the chill, the correct trend is predicted by this simple model.

According to the mechanisms of heterogeneous nucleation, the orientation of the grains formed at the surface of the chill should be random. However, as the growth proceeds and eliminates the 'poorly' oriented grains, the orientation distribution should become closer to a ⟨100⟩ crystallographic texture. Figure 6 shows the measured and simulated evolutions of the ⟨100⟩ pole figures for the same Inconel X750 specimen. The centre of the pole figures corresponds nearly to the perpendicular to the copper chill surface. The experimental and simulated pole figures were obtained using an automatic indexing of electron backscattered diffraction patterns and the 3D growth model, respectively (Gandin *et al.* 1995). As can be seen, the crystallographic orientation of the grains is nearly random near the surface of the chill and is close to a ⟨100⟩ texture 2 mm from the chill. The most probable ⟨100⟩ orientation of the dendrite trunks at this distance was

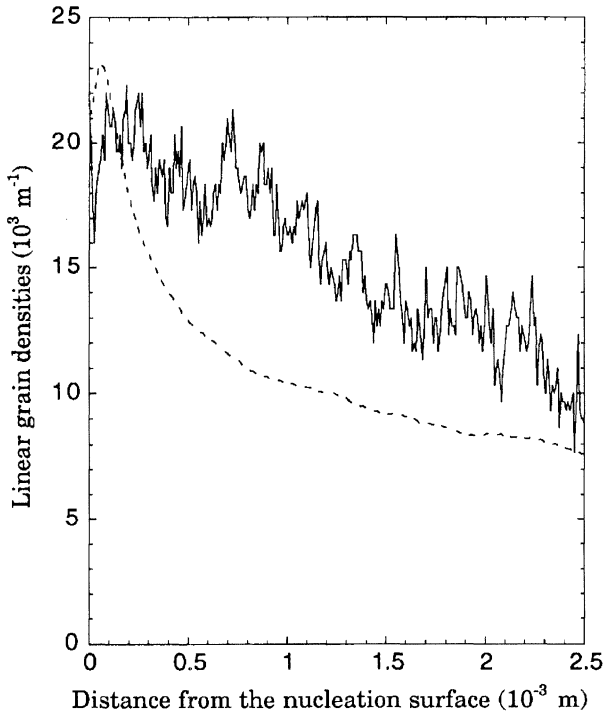

Figure 5. Measured (solid line) and calculated (dashed line) evolutions of the grain density in the columnar zone of an Inconel X750 alloy (Gandin *et al.* 1995).

calculated to be about 12° from the normal to the chill surface, a value which is very close to the experimental result.

4. Micro- and macroscopic modelling

(*a*) *Principles*

The simulation results presented in § 3 *d* have been obtained with the 3D stochastic model under the assumption of a uniform temperature. However, in most practical situations, the thermal gradient within the specimen must be considered. Since the thermal diffusion layer is much larger than the scale of the microstructure, the heat flow equation should not be solved at the scale of the CA network but rather at a coarser scale (see figure 7). For that purpose, a 2D CA algorithm has been coupled with the FE heat flow code 3-MOS (Gandin & Rappaz 1994). This code is based upon an enthalpy formulation and an implicit time-stepping scheme (Thévoz *et al.* 1990). Using a linearization procedure, the variation of enthalpies, δH_i, during one time-step can be found at all the nodal points of the FE mesh. For the nodes located in the solidifying alloy, the δH_i variations are converted into specific heat, $c_p \delta T_i$, and latent heat contributions, $L \delta f_{s,i}$, using the finer CA network and the CA algorithm.

The known temperatures at time t, T_i^t, and variations of enthalpies, δH_i, at the FE nodes are first interpolated for each CA cell, ν. Knowing these entities, the CA algorithm is applied for the nucleation/growth of the grains. For each cell, several situations can be encountered: (i) the cell was liquid and remains liquid

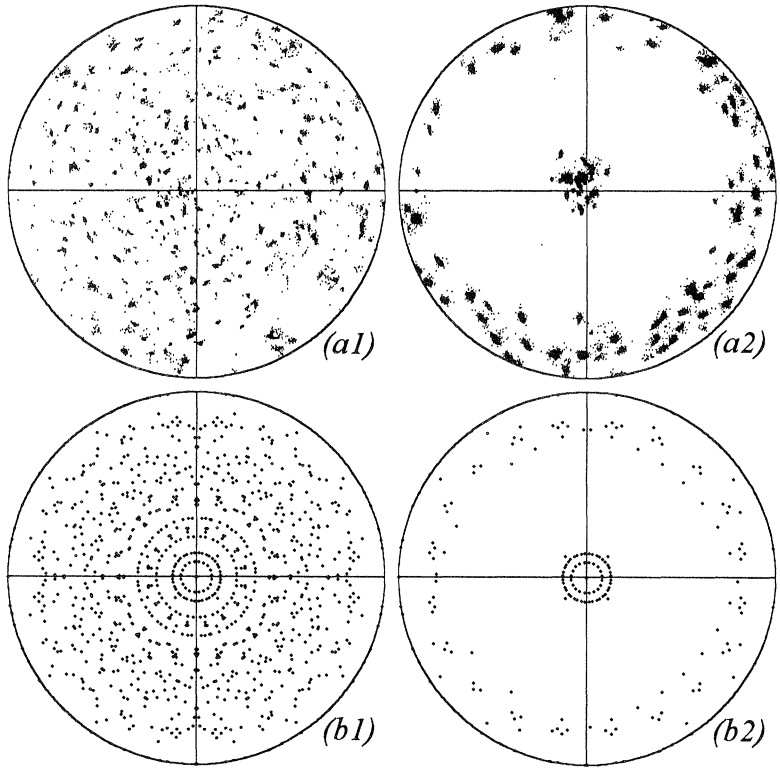

Figure 6. (*a*) Measured and (*b*) predicted ⟨100⟩ pole figures of an Inconel X750 superalloy near the surface of (1) and at 2 mm from (2) the surface of the chill. The centre of the stereographic projection corresponds to the normal to the chill surface (Gandin *et al.* 1995).

or it was already fully solid; (ii) the cell was liquid and it becomes mushy by nucleation or capture of a growing grain (i.e. Ic_ν changes from zero to a positive value); (iii) the cell was mushy but not fully solid. To each case is associated a variation of the internal volume fraction of the cell, $\delta f_{\mathrm{s},\nu}$. Once the $\delta f_{\mathrm{s},\nu}$ of all the cells have been calculated using the CA, the values $\delta f_{\mathrm{s},i}$ at the FE node locations are summed up and the new temperatures $T_i^{t+\delta t}$ are then deduced according to the heat balance: $\delta H_i = c_p \delta T_i - L \delta f_{\mathrm{s},i}$.

(*b*) *Results*

Since the CAFE model is still 2D, figure 8 must be viewed as a 2D section of a blade. The grain selector has been highly idealized as a simple zigzag and an extra reservoir (riser) of molten metal at the top of the blade has been designed. Figure 8*a* shows the 2D FE enmeshment used for the heat flow computations and the enlargement view located on the left corresponds to the left corner of the bottom platform. This zoom shows both the FE enmeshment and the CA square grid, the latter being only defined for the metal part. The final grain structure calculated with the fully coupled CAFE model is shown in figure 8*b* with various grey levels. The various steps of the solidification process are shown in figures 8*c*–*i*.

Figures 8*c* and 8*d* show the temperature distribution and the grain structure at time $t = 30$ s in the bottom part of the grain selector. The temperature scale

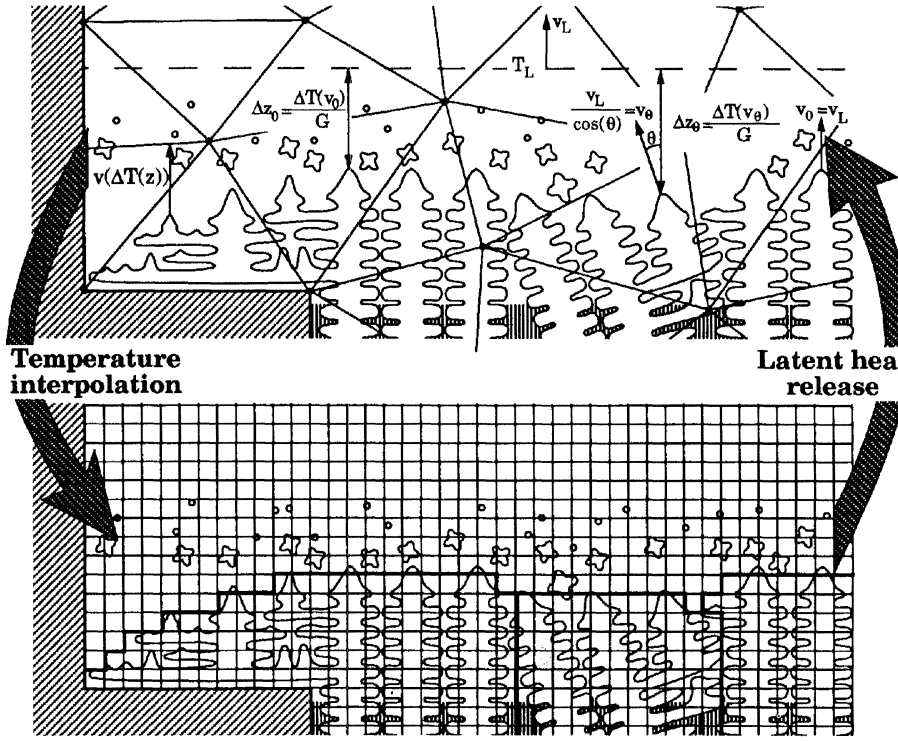

Figure 7. Coupling of the CA algorithm with FE heat flow computations.

was chosen so as to reveal the position of the liquidus front ($T_L = 1312\,^\circ$C) and to give an indication of the thermal gradient. From the many grains nucleated at the surface of the chill, only two grains remain after the zigzag of the selector (figure 8*e*, $t = 230$ s). Since most of the heat flow still goes through the grain selector, the isotherms are curved and the dendrite fronts of both grains are convex.

At time $t = 320$ s, the liquidus temperature is already above the first platform on the right of the blade and the left corner of the platform is also cooled below T_L (figure 8*f*). Since the dendritic network has to propagate in these open regions of liquid, the grain structure has the morphology shown in figure 8*g*. However, before the grain can reach the end of the platform on the right, a new grain has nucleated at this place. At time $t = 400$ s (figure 8*h*), the right part of the platform is already filled by the dendrites but another stray crystal has nucleated at the left of the platform. The liquidus isotherm, T_L, is outlined by a nearly horizontal line and is already located within the airfoil.

Figure 8*i* is an enlargement of the final grain structure calculated in the airfoil. The ⟨10⟩ crystallographic orientation of the two crystals is indicated with arrows: the grain at the left has a misorientation of -14° with respect to the vertical axis of the blade whereas that of the right grain is $+14^\circ$. The position of the liquidus isotherm is also plotted on this figure for three different times of solidification. As can be seen, the liquidus front which was slightly convex at the exit of the first platform becomes flat and then concave as solidification proceeds. This change in

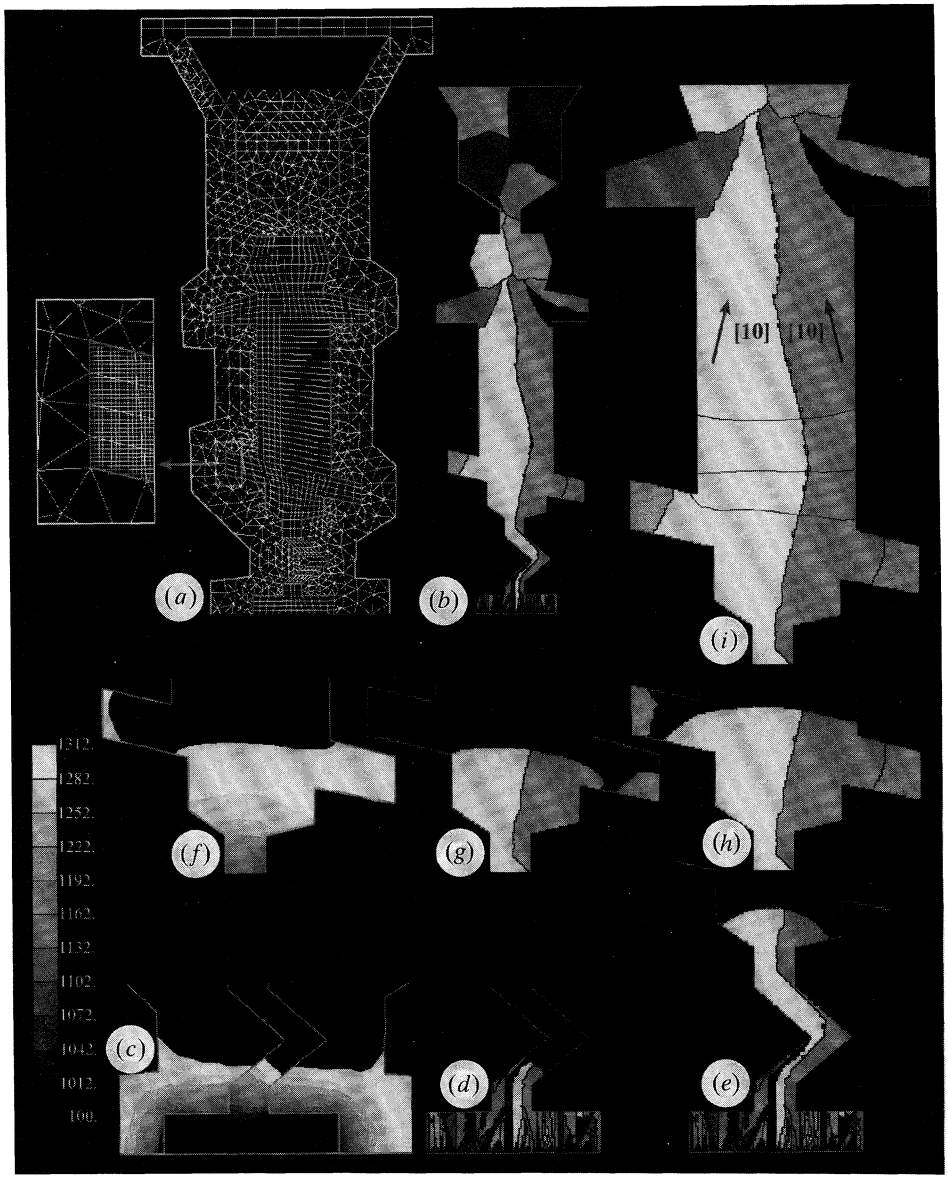

Figure 8. (*a*) Enmeshment, (*b*), (*d*), (*e*), (*g*), (*h*), (*i*) grain structure and (*c*), (*f*) temperature maps during and after solidification of an idealized 2D turbine blade.

the thermal gradient direction has a direct influence on the shape of the boundary between these two grains.

5. Conclusion

Although the full CAFE model presented here is still 2D, it brings valuable insights into the mechanisms of grain structure formation in various solidification processes. The grain selection mechanisms in the columnar zone of DS turbine blades, the transition from columnar-to-equiaxed structures, the formation of

PHILOSOPHICAL TRANSACTIONS OF THE ROYAL SOCIETY A MATHEMATICAL, PHYSICAL & ENGINEERING SCIENCES

stray crystals at section changes of the mould, the influence of the thermal gradient direction on the shape of the grain boundaries have been demonstrated for an investment cast turbine blade.

To use the full capability of the coupled CAFE model, it is necessary to extend it to three dimensions. Such an extension has been done under the limitation of uniform temperature situations (Gandin *et al.* 1993, 1994, 1995) and already has brought quantitative answers regarding the evolution of the grain density and texture. The full 3D CAFE model will be an important simulation tool for the optimization of the grain selector shape, of the casting conditions and of the yield rate of complex investment cast components.

The authors thank Dr Ph. Thévoz and Dr H. Combeau for providing figures 1 and 2 and the Commission pour l'Encouragement de la Recherche Scientifique (CERS), Bern, for its financial support.

References

Anderson, M. P., Srolovitz, D. J., Grest, G. S. & Sahni, P. S. 1984 Computer simulation of grain growth. I. Kinetics. *Acta metal.* **32**, 783–791.

Bennon, W. D. & Incropera, F. P. 1987 A continuum model for momentum, heat and species transport in binary solid–liquid phase change systems. *Int. J. Heat Mass Transfer* **30**, 2161–2187.

Chalmers, B. 1964 *Principles of solidification.* New York: Wiley.

Combeau, H. & Lesoult, G. 1993 Simulation of freckles formation and related segregation during directional solidification of metallic alloys. In *Modeling of casting, welding and advanced solidification processes VI* (ed. T. S. Piwonka *et al.*), pp. 201–208. The Minerals, Metals and Materials Society.

Ganesan, S. & Poirier, D. R. 1990 Conservation of mass and momentum for the flow of interdendritic liquid during solidification. *Metall. Trans.* B **21**, 173–181.

Gandin, Ch.-A., Rappaz, Ch. A. & Tintillier, R. 1993 Three-dimensional probabilistic simulation of solidification grain structures: application to superalloys precision castings. *Metall. Trans.* A **24**, 467–479.

Gandin, Ch.-A., Rappaz, M. & Tintillier, R. 1994 Three-dimensional simulation of the grain formation in investment casting. *Metall. Trans.* A **25**, 629–635.

Gandin, Ch.-A. & Rappaz, M. 1994 A coupled finite element–cellular automaton model for the prediction of dendritic grain structures in solidification processes. *Acta metall. mater.* **42**, 2233–2246.

Gandin, Ch.-A., Rappaz, M., West, D. & Adams, B. L. 1995 Grain texture evolution during the columnar growth of dendritic alloys. *Metall. Trans.* A **26**, 1543–1552.

Hunt, J. D. 1984 Steady state columnar and equiaxed growth of dendrites and eutectic. *Mater. Sci. Engng* **65**, 75–83.

Kobayashi, S. 1988 Solute redistribution during solidification. *J. Cryst. Growth* **88**, 87–96.

Kurz, W. & Fisher, D. J. 1989 *Fundamentals of solidification.* Aedermannsdorf: Trans. Tech. Pub.

Kurz, W., Giovanola, B. & Trivedi, R. 1986 Theory of microstructural development during rapid solidification. *Acta metall. mater.* **34**, 823–830.

Mo, A. 1994 An internal variable description of solidification suitable for macrosegregation modeling. *Metall. Trans.* B **25**, 597–605.

Ni, J. & Beckermann, C. 1991 A volume-averaged two-phase model for transport phenomena during solidification. *Metall. Trans.* B **22**, 349–361.

Rappaz, M. & Thévoz, Ph. 1987 Solute diffusion model for equiaxed dendritic growth: analytical solution. *Acta metall. mater.* **35**, 2929–2933.

PHILOSOPHICAL TRANSACTIONS OF THE ROYAL SOCIETY A MATHEMATICAL, PHYSICAL & ENGINEERING SCIENCES

Rappaz, M. 1989 Modelling of microstructure formation in solidification processes. *Int. Mater. Rev.* **34**, 93–123.

Rappaz, M. & Voller, V. 1990 Modelling of micro-macrosegregation in solidification processes. *Metall. Trans.* A **21**, 749–753.

Rappaz, M. & Gandin, Ch.-A. 1993 Probabilistic modelling of microstructure formation in solidification processes. *Acta metall. mater.* **41**, 345–360.

Sato, T., Kurz, W. & Ikawa, K. 1987 Experiments on dendrite branch detachment in the succinonitrile–canphor alloy. *Trans. Jpn Inst. Metals* **28**, 1012–1021.

Thévoz, Ph., Rappaz, M. & Desbiolles, J. L. 1990 3-MOS: a general FEM code for the prediction of microstructures in castings. In *Light metals* (ed. Ch. M. Bickert), pp. 975–984. The Minerals, Metals and Materials Society.

Toffoli, T. & Margolus, N. 1991 *Cellular automata machines.* MIT Press.

Turnbull, D. 1950 Kinetics of heterogeneous nucleation. *J. chem. Phys.* **18**, 198–203.

Voller, V. R., Brent, A. D. & Prakash, C. 1989 The modelling of heat, mass and solute transport in solidification systems. *Int. J. Heat Mass Transfer* **32**, 1719–1731.

Discussion

A. M. Stoneham (*Industrial Technology, Harwell, UK*). The end result of Professor Rappaz's very nice work is a structure (grain structure and dendrites). Some other workers have used the realizations from mesoscopic calculations to predict performance (e.g. John Harding's work on plasma-sprayed coating, where mechanical properties were predicted). Does he have plans of this sort?

M. Rappaz. Not at the moment. With the existing models of microstructure formation, the grain morphology and size, the fraction of phases, the dendrite/eutectics spacings can be calculated for as-cast components. However, the dependence of mechanical properties and performances of a component is a complex function of all these parameters. Furthermore, subsequent heat treatments (e.g. homogenization, γ' precipitation) modify the as-cast structures and the properties. The present models are therefore only one piece of the puzzle, but nevertheless essential for the process engineer.

M. McLean (*Imperial College, UK*). What material data are required to allow the models of solidification to make quantitative predictions of the microstructure that develops? Also, how sensitive are these predictions to the uncertainties in these data?

M. Rappaz. The importance of thermophysical and other materials data is not emphasized enough in the modelling community. Together with boundary conditions, they are essential in any macroscopic calculations. The present model also requires reliable phase diagram data, diffusion coefficients, surface tension, etc. in order to calculate the solidification path and the growth kinetics of the dendrites. The nucleation parameters are certainly the most critical and can only be deduced from carefully controlled experiments. This shows that simulation and experiment really go together and cannot replace each other.

M. S. Loveday (*Division of Materials Metrology, National Physical Laboratory, Teddington, UK*). Professor Rappaz has presented a very interesting example showing the importance of process control for the optimization of grain structure in an important technologically advanced component, i.e. a gas turbine blade. Processibility was recognized by the Department of Trade and Industry (UK)

PHILOSOPHICAL TRANSACTIONS OF THE ROYAL SOCIETY A MATHEMATICAL, PHYSICAL & ENGINEERING SCIENCES

as an important area when new research programmes were initiated about two years ago. There are now several research projects underway aiming to produce data of the appropriate precision for use in process control models, or to develop standard methodology for the procurement of such data. Projects are underway at the National Physical Laboratory, the National Engineering Laboratory, AEA Technology and the IRC Birmingham/Swansea to address problems such as (i) Measurement of heat capacities, enthalpies, melting ranges, densitites, viscosities, surface tension and thermal conductivities for commercial alloys, (ii) viscosity and elasticity of polymers, (iii) phase changes, recrystallization kinetics, friction and heat transfer coefficients for rolling and forging of metals, (iv) optimization of soldered joints for the electronics industry, (v) rheology of fluid solid mixtures for moulding components, and (vi) physical and mechanical properties of liquid–solid mixtures for casting of metals.

Clearly most of the above activities have a direct relevance to the production of components many of which will see service in high-temperature structural applications. All of the projects are supervised by Industrial Advisory Committees, and it is intended to rapidly disseminate the findings to the relevant sections of industry.

PHILOSOPHICAL TRANSACTIONS OF THE ROYAL SOCIETY A MATHEMATICAL, PHYSICAL & ENGINEERING SCIENCES

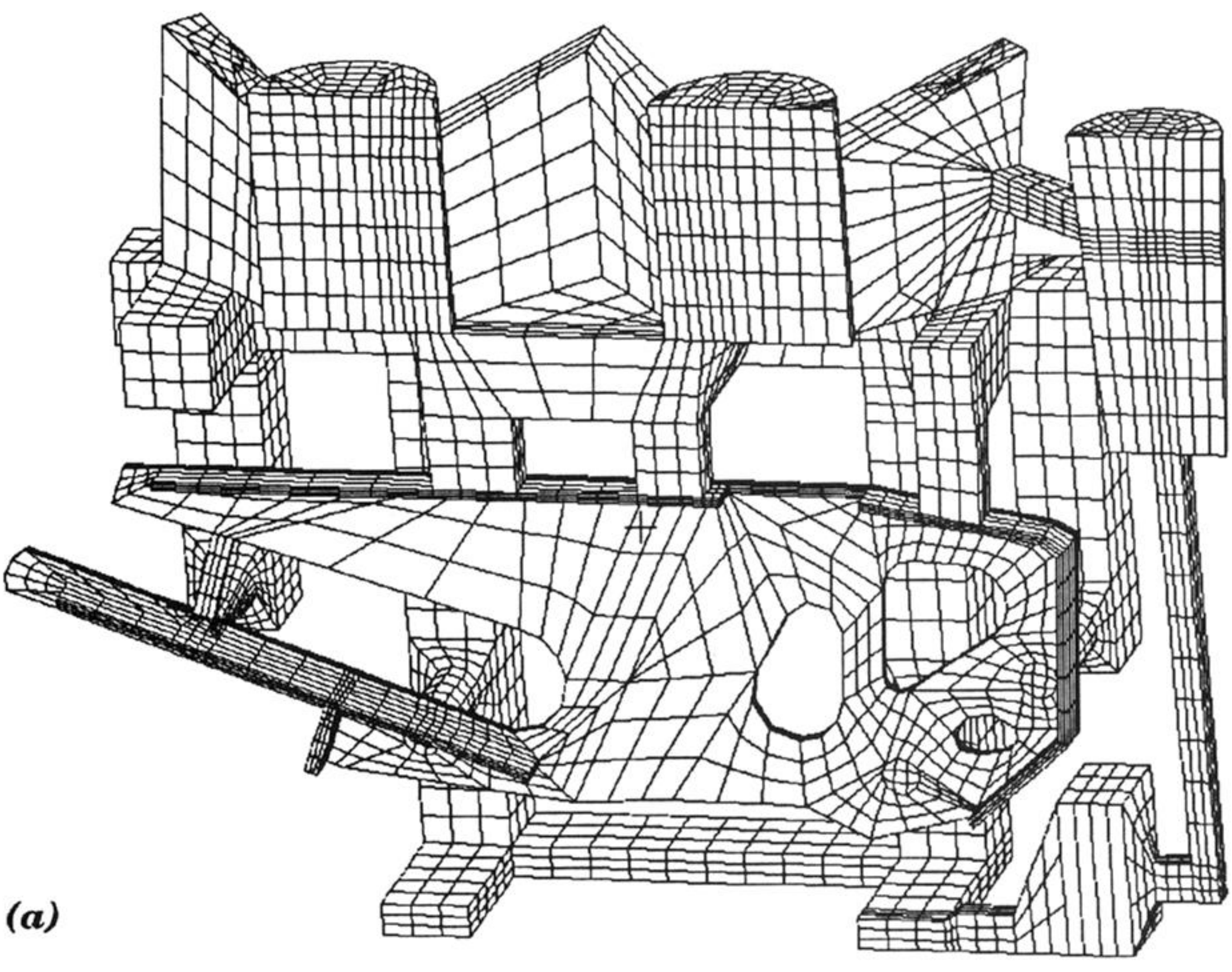

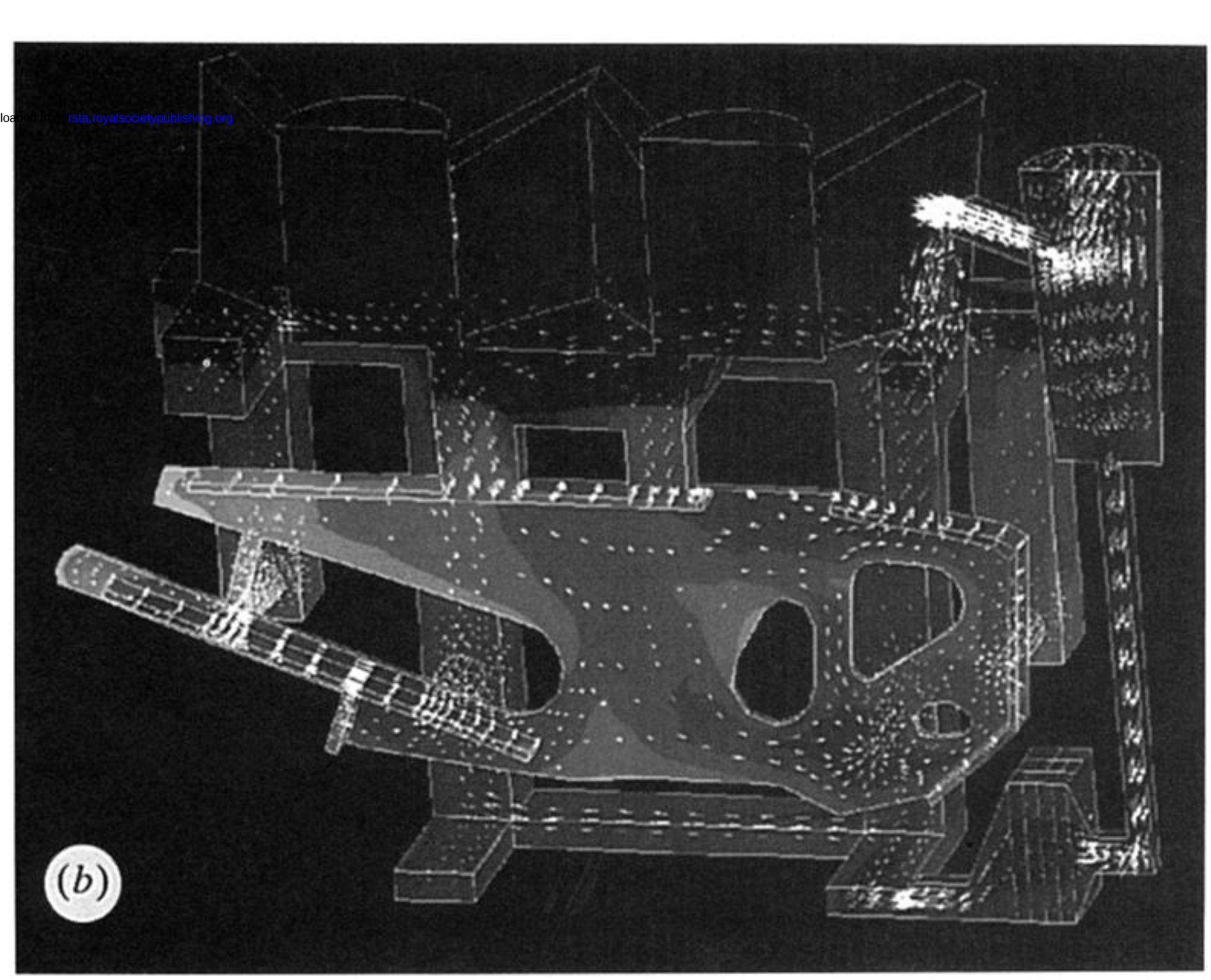

Figure 1. Structural aircraft component in Al-alloy (investment casting): (*a*) 3D enmeshment of a casting and (*b*) corresponding temperature and fluid flow velocities during mould filling (courtesy of CERCAST, calculation made with ProCAST^{TM}).

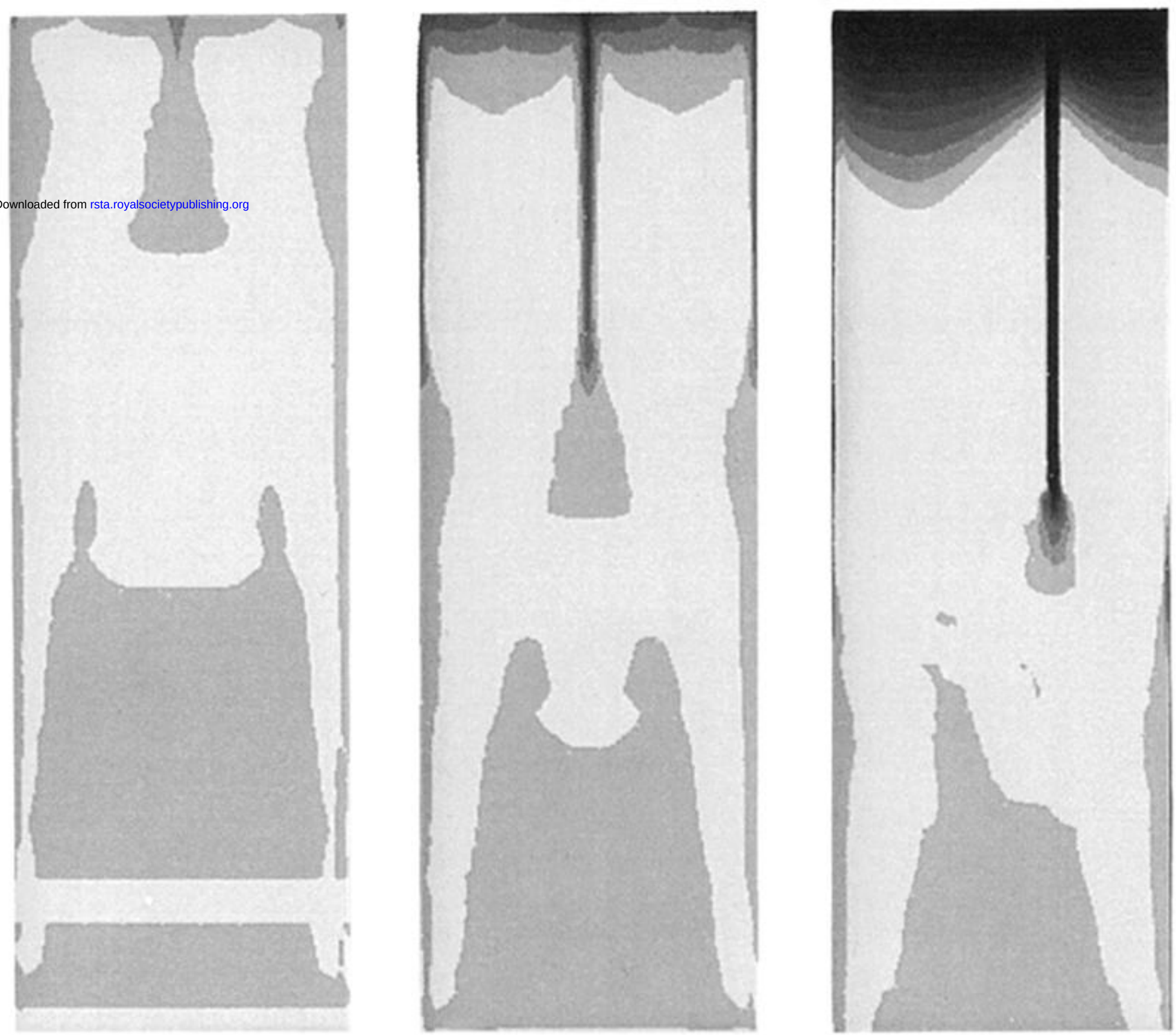

(a) (b) (c)

gure 2. 2D Al concentration distribution and freckle formation in a large Ni–Al rectangular ingot after (*a*) 1 h, (*b*) 1 h 23 min and (*c*) 8 h (courtesy of Combeau *et al.* 1993).

PHILOSOPHICAL TRANSACTIONS OF THE ROYAL SOCIETY A MATHEMATICAL, PHYSICAL & ENGINEERING SCIENCES

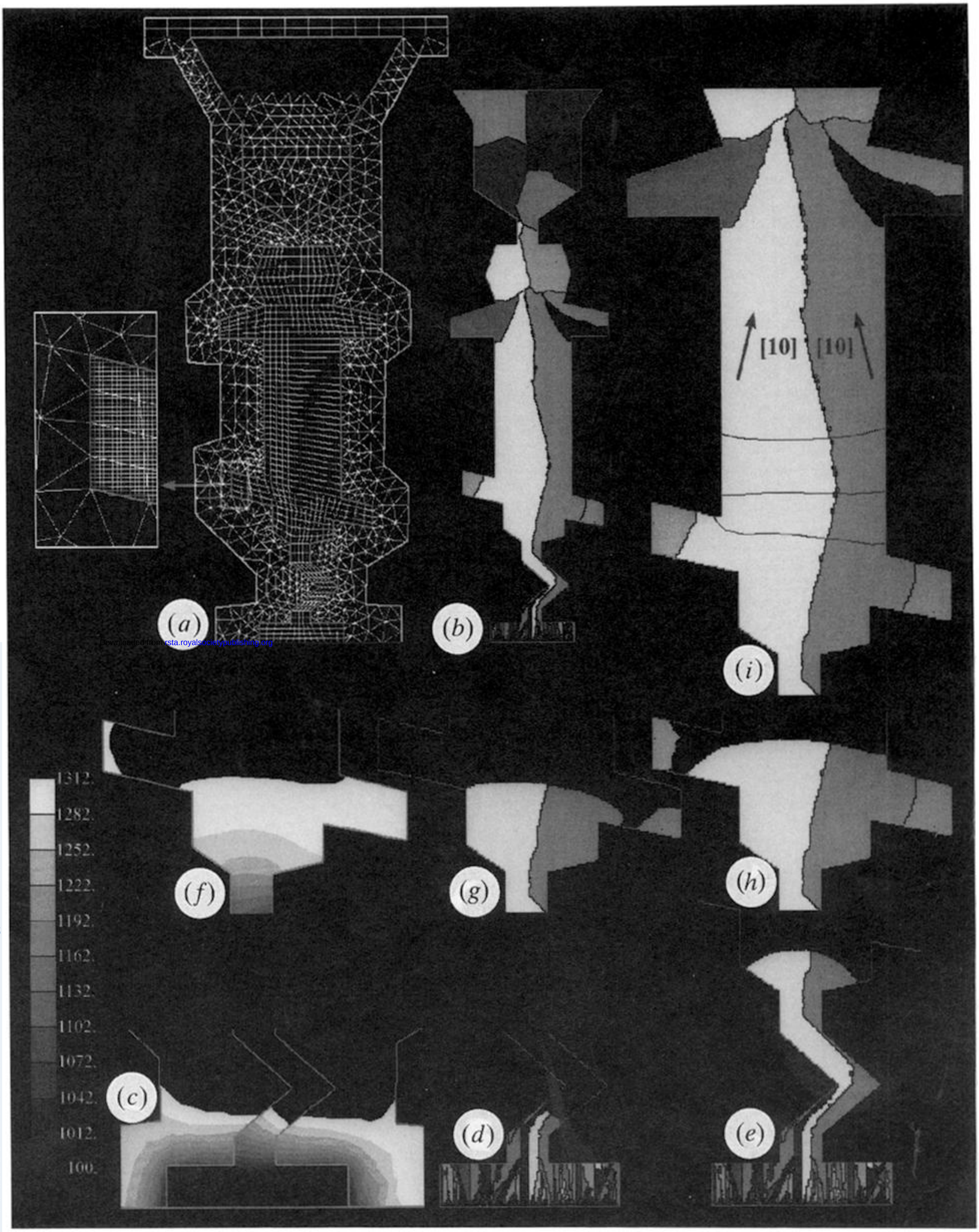

gure 8. (*a*) Enmeshment, (*b*), (*d*), (*e*), (*g*), (*h*), (*i*) grain structure and (*c*), (*f*) temperature maps during and after solidification of an idealized 2D turbine blade.